



Investigation of Heat Transfer Enhancement and Entropy Increment in a U Channel with V-shaped Ribs for Improved Hydrothermal Performance

Mohammed A. Ahmed^{1*}, Saad M. Hatem², Ibrahim K. Alabdaly³

¹ Department of Mechanical Engineering, College of Engineering, University of Anbar, Anbar 31001, Iraq

² Department of Fuel and Energy Technology Engineering, Al-Huda University College, Anbar 31001, Iraq

³ Department of Chemical and Petrochemical Engineering, College of Engineering, University of Anbar, Anbar 31001, Iraq

Corresponding Author Email: mohammed.ahmed@uoanbar.edu.iq

Copyright: ©2024 The authors. This article is published by IETA and is licensed under the CC BY 4.0 license (<http://creativecommons.org/licenses/by/4.0/>).

<https://doi.org/10.18280/ijht.420211>

ABSTRACT

Received: 26 November 2023

Revised: 8 March 2024

Accepted: 14 March 2024

Available online: 30 April 2024

Keywords:

U-form channel, heat transfer enhancement (HTE), entropy increment, V-shaped ribs

This study computationally surveyed the turbulent forced convection flow within U-form channels enhanced with V-shaped ribs, across a Reynolds number (Re) interval of 1000 to 5000. Applying the finite volume methodology, the two-dimensional governing equations of continuity, momentum, and energy were solved. The turbulent flow regime was simulated using Launder and Sharma's low Re $k-\epsilon$ model. It was found that the average Nusselt number (Nu), viscous entropy increment, heat transfer enhancement (HTE), and hydrothermal performance factor are positively correlated with both the increase in rib height and Re. Conversely, the friction factor and Bejan number (Be) demonstrated a decline as the Re increased. The optimum hydrothermal performance factor, achieving a value of 1.66, was observed in a U-form channel with a triangular rib configuration at a rib height of 1.5 mm and a Re of 5000, where the HTE ratio was recorded at 2.17. These findings suggest that U-form channels with V-shaped ribs significantly improve the hydrothermal performance of heat exchangers, enabling more compact designs. This study contributes to the body of knowledge by detailing the positive impact of rib height and flow rate on the efficiency of heat transfer mechanisms within U-form channels, highlighting potential avenues for the design of more efficient heat exchange systems.

1. INTRODUCTION

In recent years, research on varied active and passive techniques to increase the heat transfer rate (HTR) in the modern thermal systems have been become important and essential in order to cover the industry requirements. Using U-form channel with V-shaped ribs have been successfully enhanced the HTR in such channel as a compared to the conventional channels. These can mix the hot fluid near the channel walls with that in the center of the channel; increase the turbulent intensity and hence improve the heat transfer. Numerous researchers have conducted numerical and experimental investigations into the effect of streamline curvature on turbulent flows in a curvilinear channel [1-7].

Sturgis and Mudawar [8] performed an experimental study on HTE in a curvilinear channel, covering a Re interval of 9000-130000. The results demonstrated an enhancement in the HTR attributable to the flow curvature in channel. Sudo and colleagues [9] conducted experimental studies on turbulent flow in a curvilinear square duct. It is observed that when the bend angle between 0° and 30°, the fluid is accelerated near the inner wall of channel and decelerated near the external wall. Yanase and colleagues [10] computationally studied the convective heat transfer in a curvilinear rectangular duct and it was seen that the HTR rises as Dean number rises. Sugiyama and colleagues [11] performed a numerical analysis of

turbulent flow through a rectangular duct with a sharp 180-degree turn based on border-fitted coordinate system. Results showed the algebraic Reynolds stress model that has been used in this study can be adopted to simulate the turbulent flow in such shape of duct. Nobari et al. [12] computationally studied on the characteristics of flow and heat transfer in a rotating U-bend channel with varied rotating angles. It is observed that the centrifugal forces are obvious and HTR an increase due to the effects of surface curvature. Xing et al. [13] simulated of the turbulent convective flow through helical-rectangular channel using SST $k-\omega$ turbulence model. The outcomes presented that the HTR rises with rising Re. Debnath et al. [14] analyzed the conduct of thermal and flow features in turbulent forced convection flow within a rectangular elbow. Numerical results showed that recirculation regions grow at every bend and this is accompanied by pressure losses. Wang et al. [15] achieved a computational study on the characteristics of fluid flows in a curvilinear pipe within a Re interval of 5000-20000. Results showed that the separation zone of border layer is expanded with increasing the value of curvature ratio. Kanikzadeh and Sohankar [16] executed a computational study of the turbulent forced convection flow through U-form ribbed channel with Re spanning from 5000 to 20000. Findings seen that the ribbed channel display best thermal performance as a compared with a smooth channel. Vasa et al. [17] computationally researched the turbulent forced

convection flow through U-form channel with triangular cross section over Re interval of 5000-30000. The results indicated that the HTE increases with an increasing value of Re. Al-Juhaishi et al. [18] conducted a computational study on the thermal-hydraulic performance of a curvilinear channel with oblique horseshoe baffles. It is observed that the assumed geometry of the curvilinear channel with horseshoe baffles can lead to an obvious enhancement in HTR compared to a smooth channel, with an improvement spanning from 2.5 to 3.8 times. Al-Juhaishi et al. [19] performed a computational study on the flow field through a curvilinear-rectangular channel with inclined baffle. Results showed using curvilinear channel with baffle can enhance the heat transfer with reasonable increase in pressure losses. Guo et al. [20] showed an experimental and computational study of turbulent forced convection flow through a 90° bend square duct. Outcomes depicted that the thermal enhancement of the 90° curvilinear pipe as a compared to that for straight pipe is 20%. Gürbüz et al. [21] achieved numerical and experimental investigations on HTE in a U-form tubular heat exchanger with fins. It is found that the rate of heat exchange improved as well as the pressure drop increased with the adding of fins. Sanga et al. [22] computationally studied on the turbulent forced convection flow in a curvilinear cavity. Results indicated that the HTR rises with the height of the curvilinear surface but is accompanied by an increase in the pressure drop penalty. Ratul et al. [23] computationally examined of HTE in a dimpled - serpentine channel over Re spanning from 5000 to 20000 and it is found that the serpentine channel with a dimpled surface displays 1.47-times enhancement in thermal effectiveness using water as working fluid.

Ko and Wu [24] computationally surveyed on turbulent forced convection flow in a curvilinear duct. The local as well as the overall entropy increment have presented and analyzed in this study. It is observed the frictional entropy increment concentrates around the zones close to the surfaces of duct, while the thermal entropy increment only obviously occurs adjacent to the external wall of the duct. Wu et al. [25] computationally surveyed the characteristics of heat transfer and entropy increment in a helical-coiled tube and the results showed that the HTE for the helical-coiled tube is 1.35–2.2 times as compared to the straight tube. In addition, the rate of viscous entropy increment increases with the curvature ratio of the coil, while decreases with decreasing Re. Korei and Benissaad [26] computationally surveyed on the entropy increment analysis and forced convection turbulent flow through a duct with 3D 90° elbow for Re spanning from 10000 into 100000. Results showed that the obvious enhancement in the HTR can be attained near the external wall as well as the minimum entropy increment is attained at Re = 100000.

The current study aims to survey the effect of V-shaped ribs on the hydrothermal effectiveness and entropy increment characteristics of turbulent flow through a U-form channel using finite volume approach. The average Nu, Be, friction factor, thermal, viscous, and total entropy increments, HTE, and thermal-hydraulic effectiveness are presented and discussed. Furthermore, streamwise, isotherms, Be, and thermal, viscous, and total entropy increments contours are considered for various Re and ribs heights.

2. PROBLEM DESCRIPTION

Figure 1 depicts the U-form channel that considered in the

current study. The channel height (H) is 8 mm, length of straight section (L) is 100 mm and curvatures radius (R) is 10 mm. Four identical V-shaped ribs have been used with rib heights are (a=0.0, 0.5, 1.0, 1.5 mm) and rib width is (w=5 mm) and the distance between the ribs of (10 mm). The walls of the channel are uniformly heated with a constant heat flux of (q=8000 W/m²). The flow is assumed to be turbulent, steady-state, two-dimensional, incompressible, and subject to a no-slip velocity border condition along the U-channel walls. The flow at the channel inlet is considered fully-developed and pure water is employed as the working fluid in the current study.

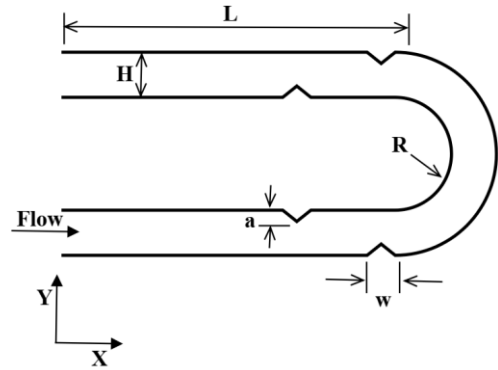


Figure 1. Geometry of present investigation

3. GOVERNING EQUATIONS AND BOUNDARY CONSTRAINTS

The governing equations may be mathematically represented in Cartesian coordinates as follows [27]:

Continuity equation:

$$\frac{\partial u}{\partial x} + \frac{\partial v}{\partial y} = 0 \quad (1)$$

u-momentum equation:

$$\begin{aligned} \frac{\partial}{\partial x}(\rho u u) + \frac{\partial}{\partial y}(\rho u v) &= -\frac{\partial p}{\partial x} + \frac{\partial}{\partial x} \left[\mu_{eff} \frac{\partial u}{\partial x} \right] \frac{\partial}{\partial y} \left[\mu_{eff} \frac{\partial u}{\partial y} \right] \\ &+ \frac{\partial}{\partial x} \left[\mu_{eff} \frac{\partial u}{\partial x} - \frac{2}{3} \rho k \right] \\ &+ \frac{\partial}{\partial y} \left[\mu_{eff} \frac{\partial v}{\partial x} \right] \end{aligned} \quad (2)$$

v-momentum equation:

$$\begin{aligned} \frac{\partial}{\partial x}(\rho u v) + \frac{\partial}{\partial y}(\rho v v) &= -\frac{\partial p}{\partial y} + \frac{\partial}{\partial x} \left[\mu_{eff} \frac{\partial v}{\partial x} \right] + \\ &\frac{\partial}{\partial y} \left[\mu_{eff} \frac{\partial v}{\partial y} \right] + \frac{\partial}{\partial x} \left[\mu_{eff} \frac{\partial u}{\partial y} \right] + \frac{\partial}{\partial y} \left[\mu_{eff} \frac{\partial v}{\partial y} - \frac{2}{3} \rho k \right] \end{aligned} \quad (3)$$

Energy equation:

$$\begin{aligned} \frac{\partial}{\partial x}(\rho u T) + \frac{\partial}{\partial y}(\rho v T) &= \frac{\partial}{\partial x} \left[\left(\frac{\mu}{Pr} + \frac{\mu_t}{Pr_t} \right) \frac{\partial T}{\partial x} \right] \\ &+ \frac{\partial}{\partial y} \left[\left(\frac{\mu}{Pr} + \frac{\mu_t}{Pr_t} \right) \frac{\partial T}{\partial y} \right] \end{aligned} \quad (4)$$

The current investigation involves the computation of turbulent-dynamic viscosity utilising the Sharma and Launder (k-ε) turbulence model. Hence, the mathematical representation of turbulent eddy viscosity may be expressed as shown [28]:

$$\mu_t = C_\mu f_\mu \rho \frac{k^2}{\varepsilon} \quad (5)$$

Turbulent kinetic energy (k) equation [24]:

$$\begin{aligned} \frac{\partial}{\partial x}(\rho uk) + \frac{\partial}{\partial x}(\rho vk) \\ = \frac{\partial}{\partial x} \left[\Gamma_k \frac{\partial k}{\partial x} \right] + \frac{\partial}{\partial y} \left[\Gamma_k \frac{\partial k}{\partial y} \right] + P_k \\ - \rho(\varepsilon + \varepsilon_w) \end{aligned} \quad (6)$$

The symbol ε_w denotes the rate of dissipation of the U-form channel, as shown by the data presented.

$$\varepsilon_w = 2 \frac{\mu}{\rho} \left[\left(\frac{\partial \sqrt{k}}{\partial x} \right)^2 + \left(\frac{\partial \sqrt{k}}{\partial y} \right)^2 \right] \quad (7)$$

The equation of turbulent kinetic energy dissipation (ε) can be given by [28]:

$$\begin{aligned} \frac{\partial}{\partial x}(\rho u \varepsilon) + \frac{\partial}{\partial y}(\rho v \varepsilon) \\ = \frac{\partial}{\partial x} \left[\Gamma_\varepsilon \frac{\partial \varepsilon}{\partial x} \right] + \frac{\partial}{\partial y} \left[\Gamma_\varepsilon \frac{\partial \varepsilon}{\partial y} \right] \\ + (C_{1f_1} P_k - \rho C_{2f_2} \varepsilon) \frac{\varepsilon}{k} + \Phi_\varepsilon \end{aligned} \quad (8)$$

where,

$$\begin{aligned} \Phi_\varepsilon = 2 \mu_t \frac{\mu}{\rho} \left[\left[\left(\frac{\partial^2 u}{\partial x^2} \right)^2 + \left(\frac{\partial^2 v}{\partial x^2} \right)^2 \right] + 2 \left(\frac{\partial^2 u}{\partial x \partial y} \right)^2 + \right. \\ \left. 2 \left(\frac{\partial^2 v}{\partial x \partial y} \right)^2 + \left(\frac{\partial^2 v}{\partial y^2} \right)^2 \right] \end{aligned} \quad (9)$$

In the previous equations, the variable P_k represents the rate of developing turbulent kinetic energy, which may be expressed as follows:

$$\begin{aligned} P_k = \mu_t \left\{ 2 \left[\left(\frac{\partial u}{\partial y} \right)^2 + \left(\frac{\partial v}{\partial x} \right)^2 \right] + \left(\frac{\partial u}{\partial y} + \frac{\partial v}{\partial x} \right)^2 \right\} \\ - \frac{2}{3} \rho k \left(\frac{\partial u}{\partial x} + \frac{\partial v}{\partial y} \right) \end{aligned} \quad (10)$$

In the previously mentioned equations, the empirical constants as well as the turbulent Prandtl number have been described as follows [28]:

$$\begin{aligned} \sigma_k = 1.0, \quad \sigma_\varepsilon = 1.3, \quad Pr_t = 0.9, \quad C_1 = 1.44, \quad C_2 \\ = 1.92, \quad C_\mu = 0.09 \end{aligned} \quad (11)$$

The calculations relating to the wall-damping functions and Re of the turbulent have been carried out in the following manner [29]:

$$f_1 = 1.0 \quad (12)$$

$$f_2 = 1 - 0.3 \exp(-Re_T^2) \quad (13)$$

$$f_\mu = \exp \left[\frac{-3.4}{(1 + 0.02 Re_T)^2} \right] \quad (14)$$

$$Re_T = \frac{\rho k^2}{\varepsilon \mu} \quad (15)$$

To solve the previously governing equations, the boundary constraints are outlined in Table 1 as follows:

Table 1. Boundary constraints of U-form channel [30]

Borders	Flow BCs	Thermal BCs
Inlet	$u = u_{in}, v = 0, k = \frac{2}{3} (0.05 u_{in})^2,$ $\varepsilon = \frac{C_\mu^{3/4} k_{in}^{3/2}}{(0.07H)}$	$T = T_{in}$
Outlet	$\frac{\partial u}{\partial \xi} = 0, \quad \frac{\partial v}{\partial \xi} = 0, \quad \frac{\partial k}{\partial \xi} = 0,$ $\frac{\partial \varepsilon}{\partial \xi} = 0$	$\frac{\partial T}{\partial \xi} = 0$
Walls	$u=0, v=0, k=0, \varepsilon=0$	$\frac{\partial T}{\partial \eta} \Big _p = -\frac{q_p}{k_f}$

After solving the governing equations, some useful parameters have been estimated to survey the fluid flow and thermal fields. The local Nu may be determined by employing [31]:

$$Nu = \frac{H}{k_f} \frac{q_p}{(T_p - T_b)} \quad (16)$$

In this context, T_p denotes the temperature distribution along the surfaces, whereas T_b represents the bulk fluid temperature, which may be calculated using the following equation [31]:

$$T_b = \frac{\iint \rho v c_p T \, dA}{\iint \rho v c_p \, dA} \quad (17)$$

The determination of the average Nu involves the Nu integration across a specified inner and external surface as follows:

$$\overline{Nu} = \frac{1}{L} \int_0^L Nu \, dx \quad (18)$$

The thermal-hydraulic effectiveness, denoted as (PEC), may be mathematically represented as shown [32]:

$$PEC = \frac{(\overline{Nu}_r / \overline{Nu}_s)}{(f_r / f_s)^{1/3}} \quad (19)$$

In this article, the symbol f represents the friction factor, that may be defined as follows [32]:

$$f = \Delta p \frac{H}{L} \frac{2}{\rho u^2} \quad (20)$$

Furthermore, the average entropy increments for the thermal $\bar{S}_{thermal}$ and viscous dissipation $\bar{S}_{viscous}$ and along surfaces may be provided in the following manner [33]:

$$\bar{S}_{thermal} = \frac{k_f}{T^2} \left[\left(\frac{\partial T}{\partial x} \right)^2 + \left(\frac{\partial T}{\partial y} \right)^2 \right] \quad (21)$$

$$\bar{S}_{viscous} = \frac{\mu}{T} \left\{ 2 \left[\left(\frac{\partial u}{\partial x} \right)^2 + \left(\frac{\partial v}{\partial y} \right)^2 \right] + \left(\frac{\partial u}{\partial y} + \frac{\partial v}{\partial x} \right)^2 \right\} \quad (22)$$

Through determining the thermal conductivity and channel height in a particular approach, dimensionless numbers representing the averages of the thermal and viscous entropy increments have been determined as follows:

$$(\bar{S}_{thermal})_H = \bar{S}_{thermal} \times \frac{H^2}{k_f} \quad (23)$$

$$(\bar{S}_{viscous})_H = \bar{S}_{viscous} \times \frac{H^2}{k_f} \quad (24)$$

The average total entropy increment, expressed as a dimensionless number, may be shown in the manner as follows as well:

$$(\bar{S}_{total})_H = (\bar{S}_{thermal})_H + (\bar{S}_{viscous})_H \quad (25)$$

4. NUMERICAL ALGORITHM

The control continuity, momentum, and energy equations are discretized employing the finite volume approach after being translated from Cartesian coordinates to body-fitted curvilinear coordinates. In the governing equations, the second-order upwind scheme and the central differencing scheme have been utilized to discretize convection and diffusion, respectively. The iterative solution has been carried out using the SIMPLE approach [34]. A Computational Fluid Dynamics (CFD) code has been created employing the FORTRAN programming language in order to simulate the present problem. The computational grid was generated by solving two Poisson equations. Figure 2 depicts the computational mesh of the current study at rib height of 1.5 mm. For the purpose to achieve numerical solution convergence, the convergence criterion of 10^{-5} has been applied for all physical variables that surveyed.

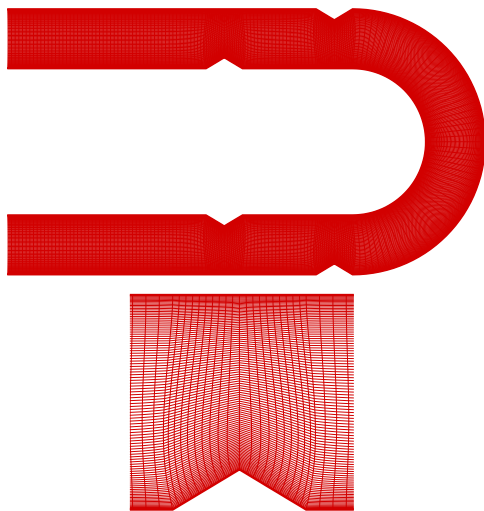


Figure 2. Computational grid of the present study at $a=1.5$, $R=10$ mm and $w=5$ mm

5. GRID INDEPENDENCE TEST AND CODE VALIDATION

The accuracy of the numerical results, as expected, is contingent on the mesh size. To explore this aspect, the average Nu has been examined across various mesh sizes within the Re interval 1000-5000 at $a=1.5$ mm (see Figure 3). It is found that the mesh size of 701×91 (701 mesh nodes in x-direction and 91 mesh nodes in y-direction) can give mesh-independent results and it is therefore adopted in the current study. The average Nu for water flowing at (293 K) in a straight channel with Re interval of (1000-5000) at constant walls temperature of (323 K) was computed and compared with the experimental results of Kilicaslan and Ibrahim Sarac [35] to validate the computationally generated CFD code in this study, as depicted in Figure 4. The findings have been observed to be in acceptable concordance. Therefore, the average deviation between the numerical results of the current study and the experimental results was approximately 10%.

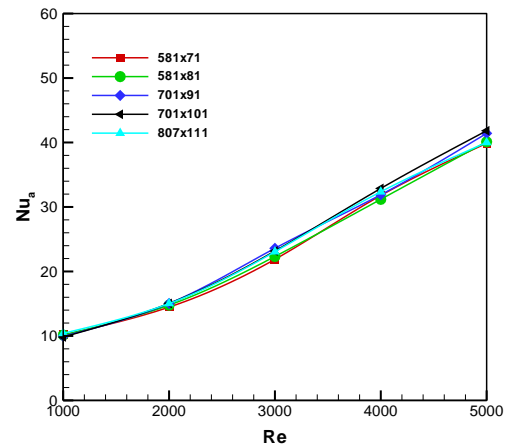


Figure 3. Effects of grid size on the average Nu at $a=1.5$, $R=10$ mm and $w=5$ mm

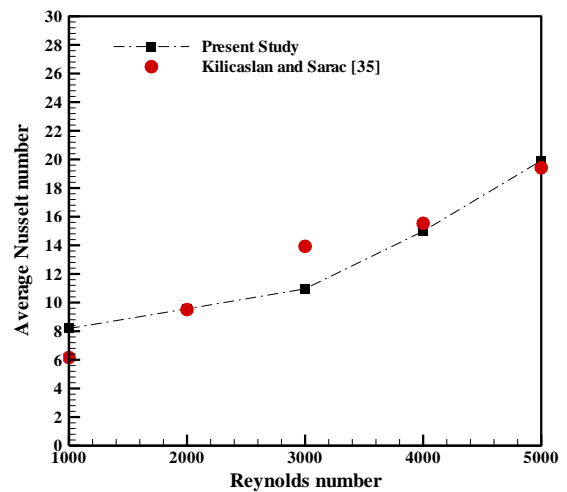


Figure 4. Comparison the present study with the previous experimental results of Kilicaslan and Ibrahim Sarac [35]

6. RESULTS AND DISCUSSION

6.1 Effects of Re

Figure 5 illustrates the streamwise contours for various Re at $a=1.5$ mm. In general, the streamwise velocity distribution

can be obviously affected by the Re. It can be seen that when the fluid flowing through the U-form channel at $Re=1000$, small vortices grow downstream the ribs near the wall of channel. As Re rises, these vortices rise in size as well as the flow become more affected and hence improve the fluid flow mixing in channel. Furthermore, the flowing of the fluid in channel with U-form curvature can provide additional enhancement in mixing of the fluid near the walls with that in centerline of channel.

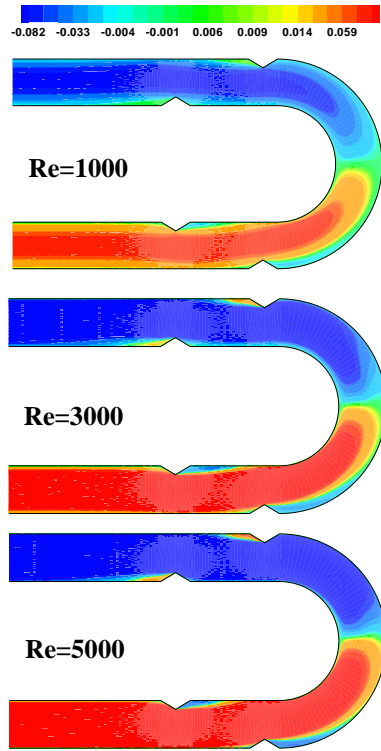


Figure 5. Streamwise contours for varied Re at $a=1.5$ mm

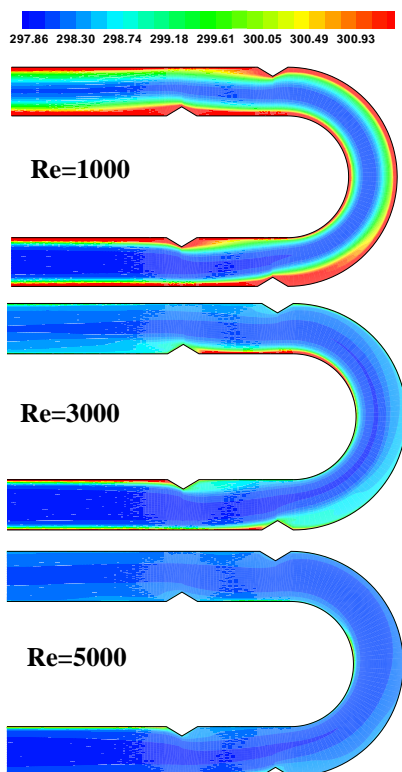


Figure 6. Isotherms contours for varied Re at $a=1.5$ mm

Figure 6 depicts the isothermal contours for various Re s at $a=1.5$ mm. It is apparent that the Re has an important influence on the thermal border layer thickness at the walls of the U-channel. With rising Re , the thickness of thermal border layer decreases, due to rise the velocity gradient at the walls of U-channel with Re . On the other hand, the presence of V-shaped ribs inside the channel causes a growing re-circulation zone downstream of the ribs, as mentioned previously, and consequently improves the hot water mixing near the walls with the colder water in the centerline of the U-channel.

Figure 7 displays the thermal entropy increment contours for varied Re at $a=1.5$ mm. It has been seen that the thermal entropy increment gradient at the channel wall increases with Re , attributed to the increase in the gradient of temperature at the U-channel wall with increasing Re . Moreover, the gradient of thermal entropy increment upstream the ribs is smaller than downstream the ribs with respect to the influence of the re-circulation regions.

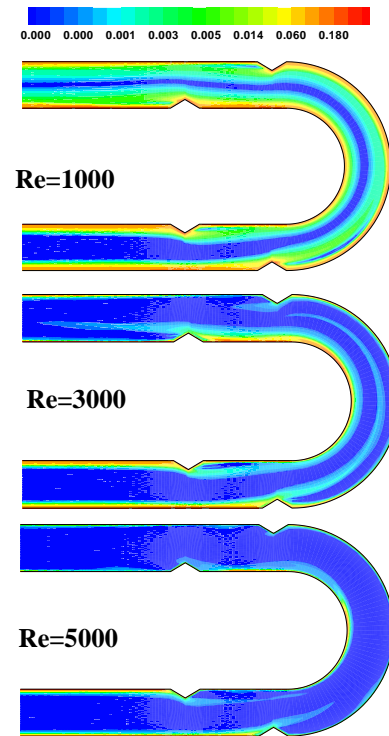
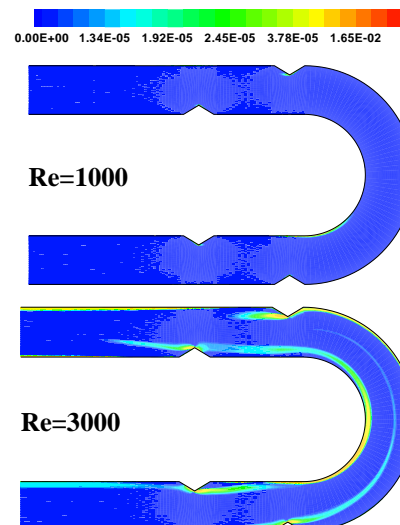


Figure 7. Thermal entropy increment contours for varied Re at $a=1.5$ mm



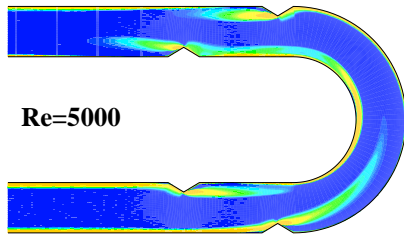


Figure 8. Viscous entropy increment contours for varied Re at $a=1.5$ mm

Figure 8 presents the viscous entropy increment contours for varied Re at $a=1.5$ mm. It can be observed that the viscous entropy rises with rising Re due to rise the frictional irreversibility with Re.

Figure 9 shows the total entropy increment contours for varied Re at $a=1.5$ mm. It is obvious that the total thermal and viscous entropy increment depend mainly on Re. In general, the behavior of total entropy increment is the same for the thermal entropy increment because of the value of thermal entropy increment is greater than the viscosity entropy increment as previously presented in Figures 6 and 7. Also, it is found that the gradient of the total entropy increment at the U-channel wall rise as Re rises due to increase the gradient of thermal entropy increment with Re, as depict in Figure 7.

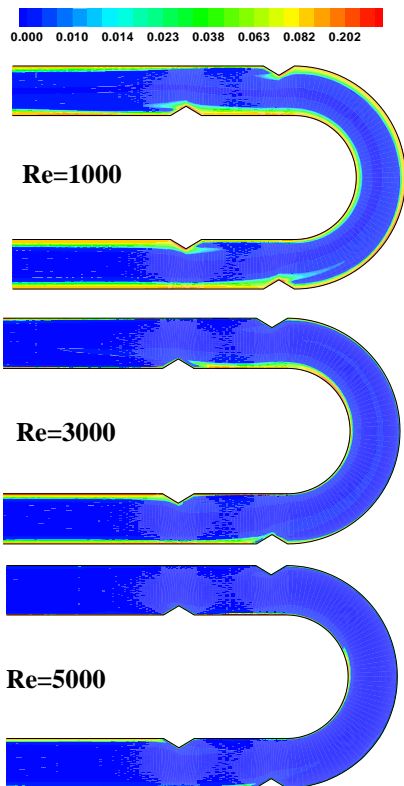


Figure 9. Total entropy increment contours for varied Re at $a=1.5$ mm

6.2 Effect of rib heights

Figure 10 presents the streamwise velocity contours for various rib heights ($a=0, 1.0, 1.5$ mm) at $Re=3000$. With ribs addition, the re-circulation zones develop downstream of the V-shaped ribs which lead to enhance the fluid flow mixing in

U- channel. As the ribs height increase, the size and intensity of these vortices increase, resulting improve the fluid mixing. Moreover, the fluid flow velocity in the core of U-channel rises with rising ribs height due decrease the spacing between the top and bottom walls. Figure 11 illustrates the isothermal contours for various rib heights ($a=0, 1.0, 1.5$ mm) at $Re=3000$. As the rib height increase, the thickness of thermal border reduces due to the effect of re-circulation zones that develop behind the ribs. These zones work to fluid mixing and thus lead to decrease the thickness of thermal border layer and consequently HTE.

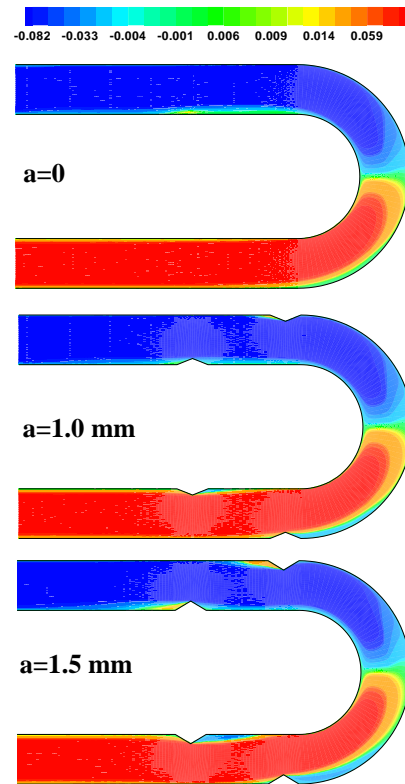


Figure 10. Streamwise velocity contours for varied rib height at $Re=3000$

Figure 12 depicts the thermal entropy increment contours for varied rib heights ($a=0, 1.0, 1.5$ mm) at $Re=3000$. It is observed that the thermal entropy increment gradient at the walls of channel rises with rising ribs height owing to a growth the thermal border layer gradient as shown in Figure 11. This is because presence of the re-circulation zones that developed downstream the ribs can improve fluid flow mixing in channel. Figure 13 presents the viscous entropy increment contours for varied rib heights ($a=0, 1.0, 1.5$ mm) at $Re=3000$. It is apparent that viscous entropy increment increase as the rib height increase, attributed to the enlargement of recirculation regions with rib height, consequently as a result a rise in frictional irreversibility. Figure 14 demonstrates the total entropy increment contours for varied rib heights ($a=0, 1.0, 1.5$ mm) at $Re=3000$. With increasing ribs height, the total entropy increment decrease due to it depends on the thermal entropy increment as shown in Figure 12. Because of the decrease in the thickness of thermal border layer as well as the re-circulation regions that presence downstream of the ribs which works on cold water mixing in the core of U-channel with hot water near the channel walls.

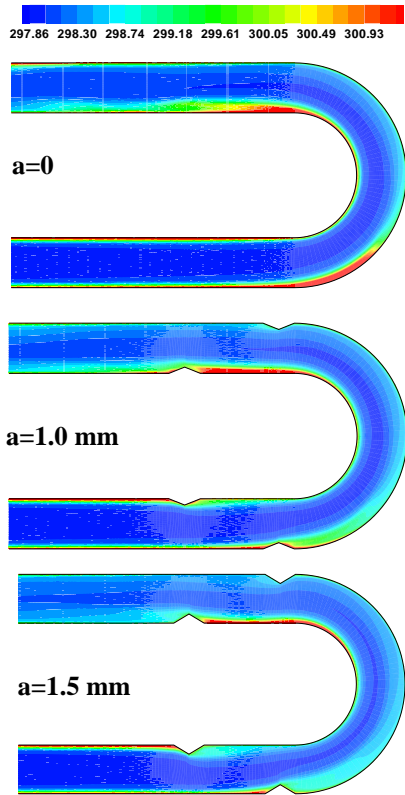


Figure 11. Isotherms contours for varied Rib height at $Re=3000$

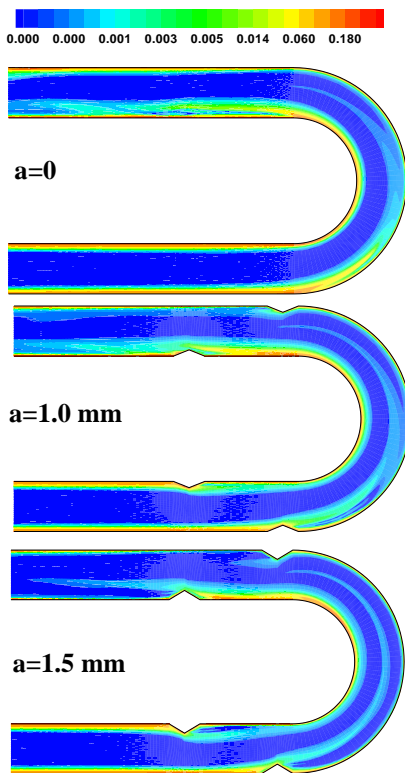


Figure 12. Thermal entropy increment contours for varied Rib height at $Re=3000$

Figure 15 illustrates the relationship between the average Nu and Re for various rib heights. In general, for all rib heights, the average Nu shows an increase with Re , as predicted. As rib heights increase, the average Nu increases due to the expansion of re-circulation zones that present downstream of

the ribs which improve the fluid flow mixing inside the U-channel and hence rise the HTR. This finding agrees with the computational study of the Manca et al. [30] and Salameh and colleagues [36].

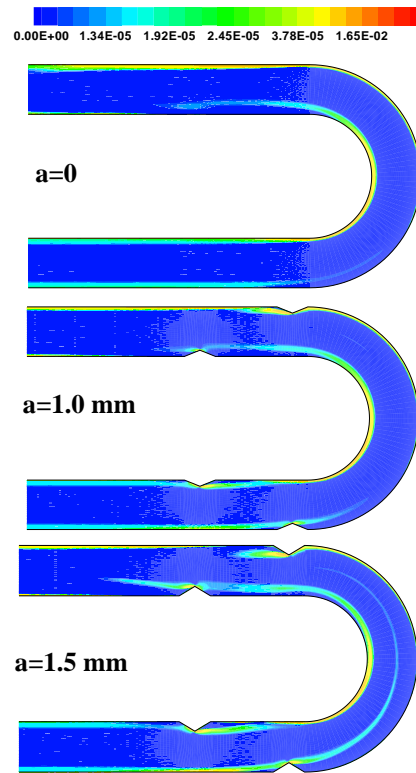


Figure 13. Viscous entropy increment contours for varied Rib height at $Re=3000$

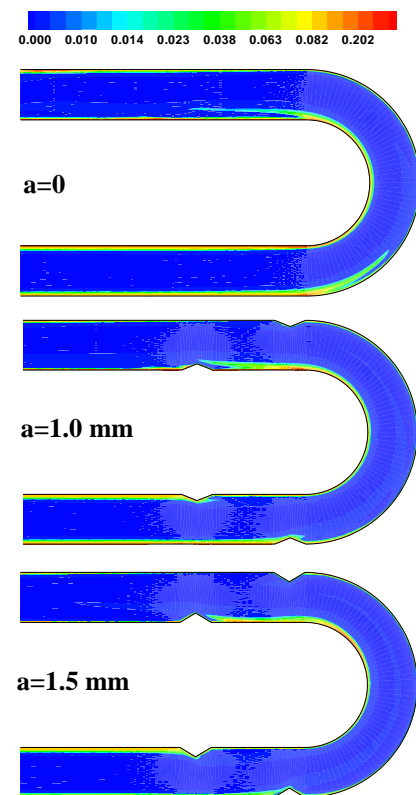


Figure 14. Total entropy increment contours for varied Rib height at $Re=3000$

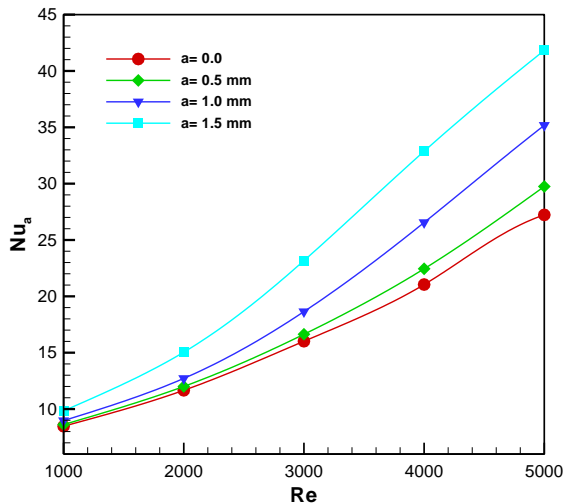


Figure 15. Variation of the average Nu with Re for varied rib heights on PEC at R=10 mm and w=5 mm

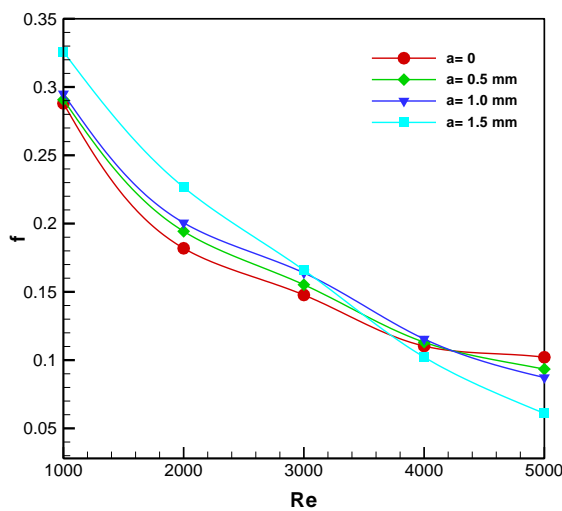


Figure 16. Variation of friction factor with Re for varied rib heights on PEC at R=10 mm and w=5 mm

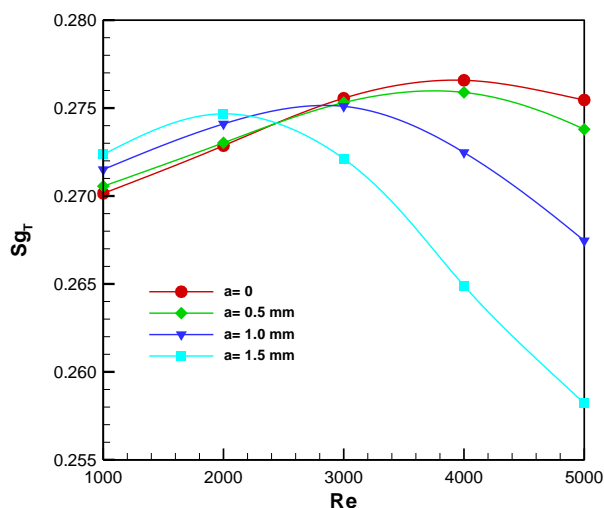


Figure 17. Variation of thermal entropy increment with Re for varied rib heights on PEC at R=10 mm and w=5 mm

Figure 16 illustrates the friction factor versus Re for various rib heights. For all rib heights, it is obvious that the friction factor decreases with a rise in Re. This result corresponds with the experimental result of Salameh and colleagues [36]. As rib

heights increases, the friction factor increases when $Re \leq 3000$. This indicates that at lower Res, the presence of ribs leads to raised frictional losses. While the friction decreases as rib heights rises when $Re > 4000$.

Figure 17 depicts the thermal entropy increment versus Re for various rib heights. It has been found that the thermal entropy increment gradually decreases with rising Re ($Re > 3000$) and rib height. As a result of the presence of ribs that create a recirculation zone, which in turn improves fluid mixing and reduces the thermal border layer thickness as well as the irreversibility of heat transfer, as shown in Figures 7 and 12. Furthermore, the smooth U-bend channel ($a=0$) provided the greatest thermal entropy increment compared with other cases. This happens due to poor fluid mixing and hence increase the thickness of thermal border layer.

Figure 18 demonstrates the viscous entropy increment versus Re for various rib heights. It is found that with rising Re and rib heights, the viscous entropy increment rises due to a rise in the irreversibility of viscous entropy increment in U-bend channel. Therefore, the maximum viscous entropy increment happens at a higher Re and higher rib height.

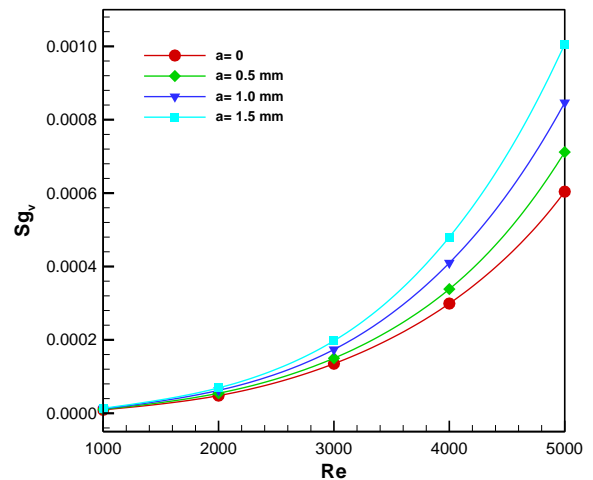


Figure 18. Variation of viscous entropy increment with Re for varied rib heights on PEC at R=10 mm and w=5 mm

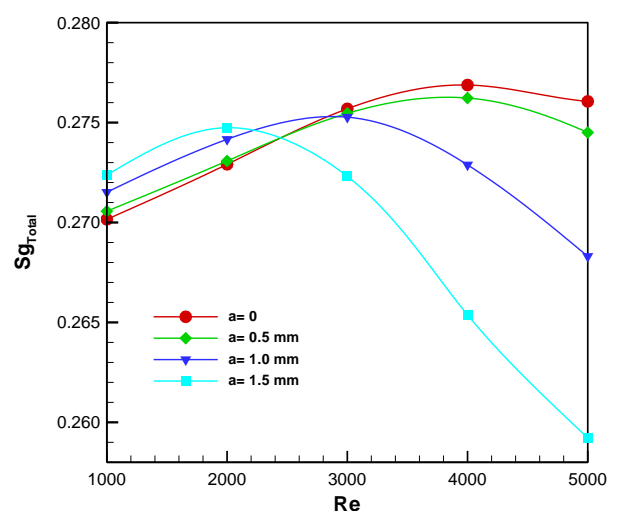


Figure 19. Variation of total entropy increment with Re for varied rib heights on PEC at R=10 mm and w=5 mm

Figure 19 shows the total entropy increment versus Re for various rib heights. It can be noted that the total entropy increment rises when $Re \leq 2000$, while it decreases gradually

with increasing Re when $Re \geq 4000$. This behavior is same for the thermal entropy increment, see Figure 17. In the other word, the influence of thermal entropy increment is more dominate than the viscous entropy.

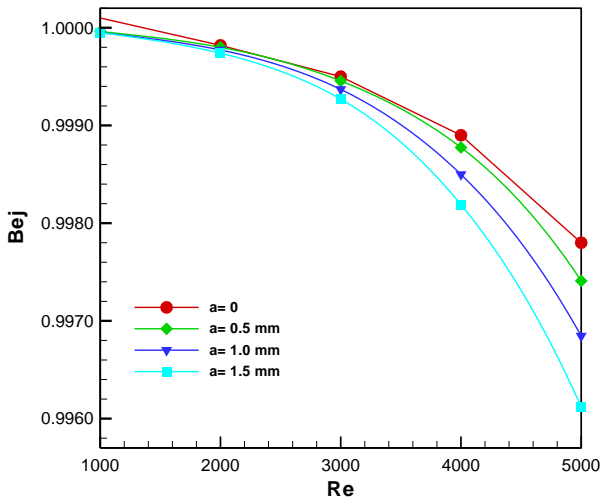


Figure 20. Variation of Bejen number with Re for varied rib heights on PEC at R =10 mm and w= 5 mm

Figure 20 depicts the Be versus Re for various rib heights. In general, it can be observed that Be, which indicates the ratio of heat transfer irreversibility to total entropy increment, is gradually decreased with increasing Re. With increasing rib heights, the Be decreases. This is because, with an increase in rib heights, the flow becomes more intricate, resulting in elevated frictional entropy increment and consequently reduce the Be.

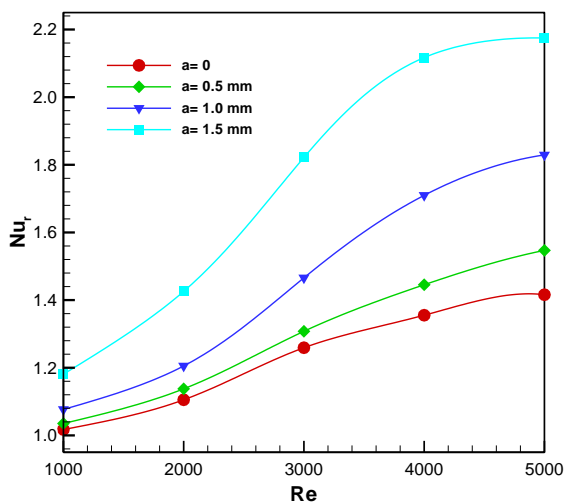


Figure 21. Variation of heat transfer enhancement with Re for varied rib heights on PEC at R=10 mm and w=5 mm

Figure 21 displays the ratio of the Nu for U-channel with rib to that for the straight channel without rib versus Re for varied rib heights. For a given rib height, it is found the enhancement ratio rises as Re rises. Also, the enhancement ratio rises as the rib height rises. This is due to when the rib height rise, the size of re-circulation region increases and hence rise the HTR as a result enhance the fluid flow mixing in U-channel. Therefore, the maximum value of enhancement ratio is approximately 2.17 which attained at a=1.5 mm and Re=5000.

Figure 22 presents the variation of thermal-hydraulic

effectiveness factor (PEC) with Re for various rib heights. For a given rib height, it can be noted that the effectiveness factor rises with Re. It is observed that rib height has a clear influence on the effectiveness factor. At low Re, there is a slight increase in the effectiveness factor with increasing the rib height. However, this effect increases as Reynolds increase since the fluid mixing is improved with rising Re. Also, it is noticed that the value of (PEC) is less than unity when a= 0 and 0.5 mm for all values of Re. This demonstrates that the increasing in the friction losses is the higher than the improvement in heat transfer. In addition, value of PEC is greater than one when Re is greater than 3000 and a=1 and 1.5 mm. The highest value of (PEC) is approximately 1.66 occurs at Re=5000 and a=1.5 mm. It can be concluded that the optimal selection for rib height is a=1.5 mm.

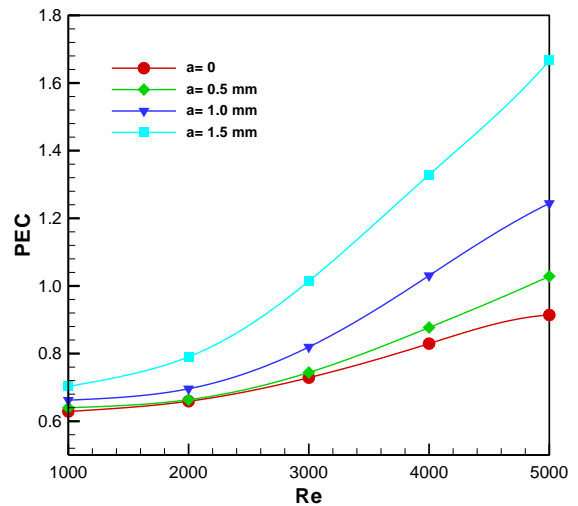


Figure 22. Variation of PEC with Re for varied rib heights on PEC at R =10 mm and w=5 mm

7. CONCLUSION

In the current investigation, turbulent forced convection flow through U-form channel with triangular rib has been computationally analyzed employing finite volume approach for rib height of (0, 0.5, 1.0, 1.5 mm) and Re spanning from 1000 to 5000. The effect of Re as well as rib height on the thermal and fluid flow characteristics are presented and surveyed. Findings showed that the average Nu, viscous entropy increment, HTE, thermal-hydraulic effectiveness factor increase with the rib height and Re. While, the friction factor and be decreases as Re increases. Furthermore, the peak value of PEC is 1.66 achieved using U-form channel with triangular rib at rib height of 1.5 mm and Re of 5000 and corresponding HTE is 2.17. However, designing of heat exchanger using U-form channel with triangular rib can provide the best effectiveness with more compact design.

REFERENCES

- [1] Wattendorf, F.L. (1935). A study of the effect of curvature on fully developed turbulent flow. Proceedings of the Royal Society of London. Series A-Mathematical and Physical Sciences, 148(865): 565-598. <https://doi.org/10.1098/rspa.1935.0034>
- [2] Bradshaw, P., Young, A.D. (1973). Effects of streamline

- curvature on turbulent flow. *AGARDograph*, 169.
- [3] Gibson, M.M. (1985). Effects of streamline curvature on turbulence. In *Frontiers in Fluid Mechanics: A Collection of Research Papers Written in Commemoration of the 65th Birthday of Stanley Corrsin*, Berlin, pp. 184-198.
- [4] Cheng, G.C., Farokhi, S. (1992). On turbulent flows dominated by curvature effects. *Journal of fluid Mechanics*, 114: 52-57. <https://doi.org/10.1115/1.2909999>
- [5] Miranville, A. (1997). Effects of curvature on flows in a curved channel. *Applicable Analysis*, 66(3-4): 247-260. <https://doi.org/10.1080/00036819708840585>
- [6] Rao, D.V., Babu, C.S., Prabhu, S.V. (2004). Effect of turn region treatments on the pressure loss distribution in a smooth square channel with sharp 180° bend. *International Journal of Rotating Machinery*, 10: 459-468. <https://doi.org/10.1155/S1023621X04000454>
- [7] Iacovides, H., Jackson, D.C., Kelemenis, G., Launder, B.E., Yuan, Y.M. (1999). Experiments on local heat transfer in a rotating square-ended U-bend. *International Journal of Heat and Fluid Flow*, 20(3): 302-310. [https://doi.org/10.1016/S0142-727X\(99\)00019-3](https://doi.org/10.1016/S0142-727X(99)00019-3)
- [8] Sturgis, J.C., Mudawar, I. (1999). Single-phase heat transfer enhancement in a curved, rectangular channel subjected to concave heating. *International Journal of Heat and Mass Transfer*, 42(7): 1255-1272. [https://doi.org/10.1016/S0017-9310\(98\)00232-4](https://doi.org/10.1016/S0017-9310(98)00232-4)
- [9] Sudo, K., Sumida, M., Hibara, H. (2001). Experimental investigation on turbulent flow in a square-sectioned 90-degree bend. *Experiments in Fluids*, 30(3): 246-252. <https://doi.org/10.1007/s003480000157>
- [10] Yanase, S.R.N.M., Mondal, R.N., Kaga, Y. (2005). Numerical study of non-isothermal flow with convective heat transfer in a curved rectangular duct. *International Journal of Thermal Sciences*, 44(11): 1047-1060. <https://doi.org/10.1016/j.ijthermalsci.2005.03.013>
- [11] Sugiyama, H., Tanaka, T., Mukai, H. (2008). Numerical analysis of turbulent flow separation in a rectangular duct with a sharp 180-degree turn by algebraic Reynolds stress model. *International Journal for Numerical Methods in Fluids*, 56(12): 2207-2228. <https://doi.org/10.1002/flid.1581>
- [12] Nobari, M.R.H., Nousha, A., Damangir, E. (2009). A numerical investigation of flow and heat transfer in rotating U-shaped square ducts. *International Journal of Thermal Sciences*, 48(3): 590-601. <https://doi.org/10.1016/j.ijthermalsci.2008.04.001>
- [13] Xing, Y., Zhong, F., Zhang, X. (2014). Numerical study of turbulent flow and convective heat transfer characteristics in helical rectangular ducts. *Journal of Heat Transfer*, 136(12): 121701. <https://doi.org/10.1115/1.4028583>
- [14] Debnath, R., Mandal, A., Majumder, S., Bhattacharjee, S., Roy, D. (2014). Numerical analysis of turbulent fluid flow and heat transfer in a rectangular elbow. *Journal of Applied Fluid Mechanics*, 8(2): 231-241. <https://doi.org/10.18869/acadpub.jafm.67.221.21363>
- [15] Wang, Y., Dong, Q., Wang, P. (2015). Numerical investigation on fluid flow in a 90-degree curved pipe with large curvature ratio. *Mathematical Problems in Engineering*, 2015: 548262. <https://doi.org/10.1155/2015/548262>
- [16] Kanikzadeh, M., Sohankar, A. (2016). Numerical investigation of forced convection flow of nanofluids in rotating U-shaped smooth and ribbed channels. *Heat Transfer Engineering*, 37(10): 840-861. <https://doi.org/10.1080/01457632.2015.1089739>
- [17] Vasa, A., Barik, A.K., Nayak, B. (2017). Turbulent convection heat transfer enhancement in a 180-degree U-bend of triangular cross-section using nanofluid. *IOP Conference Series: Materials Science and Engineering*, 225(1): 012067. <https://doi.org/10.1088/1757-899X/225/1/012067>
- [18] Al-Juhaishi, L.F., Mohd Ali, M.F., Mohammad, H.H., Ajeel, R.K. (2020). Numerical thermal-hydraulic performance investigations in turbulent curved channel flow with horseshoe baffles. *Heat Transfer*, 49(6): 3816-3836. <https://doi.org/10.1002/hjt.21810>
- [19] Al-Juhaishi, L.F.M., Ali, M.F.M., Mohammad, H.H. (2020). Numerical study on heat transfer enhancement in a curved channel with baffles. *Journal of Advanced Research in Fluid Mechanics and Thermal Sciences*, 68(2): 72-83. <https://doi.org/10.37934/arfmts.68.2.7283>
- [20] Guo, G., Kamigaki, M., Zhang, Q., Inoue, Y., Nishida, K., Hongou, H., Koutoku, M., Yamamoto, R., Yokohata, H., Sumi, S., Ogata, Y. (2020). Experimental study and conjugate heat transfer simulation of turbulent flow in a 90° curved square pipe. *Energies*, 14(1): 94. <https://doi.org/10.3390/en14010094>
- [21] Gürbüz, E.Y., Variyenli, H.İ., Sözen, A., Khanlari, A., Ökten, M. (2021). Experimental and numerical analysis on using CuO-Al₂O₃/water hybrid nanofluid in a U-type tubular heat exchanger. *International Journal of Numerical Methods for Heat & Fluid Flow*, 31(1): 519-540. <https://doi.org/10.1108/HFF-04-2020-0195>
- [22] Sanga, P.J., Kumar, A., Mishra, S.K. (2022). Numerical investigation of turbulent forced convection flow in a two-dimensional curved surface cavity. *Engineering Applications of Computational Fluid Mechanics*, 16(1): 359-373. <https://doi.org/10.1080/19942060.2021.2016491>
- [23] Ratul, R.E., Ahmed, F., Alam, S., Karim, M.R., Bhuiyan, A.A. (2023). Numerical study of turbulent flow and heat transfer in a novel design of serpentine channel coupled with D-shaped jaggedness using hybrid nanofluid. *Alexandria Engineering Journal*, 68: 647-663. <https://doi.org/10.1016/j.aej.2023.01.061>
- [24] Ko, T.H., Wu, C.P. (2009). A numerical study on entropy generation induced by turbulent forced convection in curved rectangular ducts with various aspect ratios. *International Communications in Heat and Mass Transfer*, 36(1): 25-31. <https://doi.org/10.1016/j.icheatmasstransfer.2008.08.016>
- [25] Wu, S.Y., Chen, S.J., Li, Y.R., Li, L.J. (2009). Numerical investigation of turbulent flow, heat transfer and entropy generation in a helical coiled tube with larger curvature ratio. *Heat and Mass Transfer*, 45: 569-578. <https://doi.org/10.1007/s00231-008-0458-5>
- [26] Korei, Z., Benissaad, S. (2021). Turbulent forced convection and entropy analysis of a nanofluid through a 3D 90° elbow using a two-phase approach. *Heat Transfer*, 50(8): 8173-8203. <https://doi.org/10.1002/hjt.22272>
- [27] Yang, L.C., Asako, Y., Yamaguchi, Y., Faghri, M. (1997). Numerical prediction of transitional characteristics of flow and heat transfer in a corrugated duct. *ASME Journal of Heat and Mass Transfer*, 119(1): 62-69. <https://doi.org/10.1115/1.2824101>

[28] Blazek, J. (2015). Computational Fluid Dynamics: Principles and Applications. Butterworth-Heinemann.

[29] Chen, C.J. (1997). Fundamentals of Turbulence Modelling. CRC Press.

[30] Manca, O., Nardini, S., Ricci, D. (2012). A numerical study of nanofluid forced convection in ribbed channels. Applied Thermal Engineering, 37: 280-292. <https://doi.org/10.1016/j.applthermaleng.2011.11.030>

[31] Kalteh, M., Abbassi, A., Saffar-Avval, M., Harting, J. (2011). Eulerian–Eulerian two-phase numerical simulation of nanofluid laminar forced convection in a microchannel. International Journal of Heat and Fluid Flow, 32(1): 107-116. <https://doi.org/10.1016/j.ijheatfluidflow.2010.08.001>

[32] Kock, F., Herwig, H. (2004). Local entropy production in turbulent shear flows: A high-Reynolds number model with wall functions. International Journal of Heat and Mass Transfer, 47(10-11): 2205-2215. <https://doi.org/10.1016/j.ijheatmasstransfer.2003.11.025>

[33] Kock, F., Herwig, H. (2005). Entropy production calculation for turbulent shear flows and their implementation in CFD codes. International Journal of Heat and Fluid Flow, 26(4): 672-680. <https://doi.org/10.1016/j.ijheatfluidflow.2005.03.005>

[34] Versteeg, H.K., Malalasekera, W. (2007). An Introduction to Computational Fluid Dynamics: The Finite Volume Method. Pearson Education.

[35] Kilicaslan, I., Ibrahim Sarac, H. (1998). Enhancement of heat transfer in compact heat exchanger by different type of rib with holographic interferometry. Experimental Thermal and Fluid Science, 17(4): 339-346. [https://doi.org/10.1016/S0894-1777\(98\)00006-5](https://doi.org/10.1016/S0894-1777(98)00006-5)

[36] Salameh, T., Sunden, B. (2010). An experimental study of heat transfer and pressure drop on the bend surface of a U-duct. In Proceedings of the ASME Turbo Expo 2010: Power for Land, Sea, and Air, Volume 4: Heat Transfer, Parts A and B. Glasgow, UK, pp. 13-21. <https://doi.org/10.1115/GT2010-22139>

NOMENCLATURE

a	Rib height (mm)
Be	Bejan number
C_1, C_2, C_μ	Empirical constant for turbulence model
C_p	Specific heat capacity (J/kg K)
f	Friction factor

f_1, f_2, f_μ	Damping function
H	Channel height (mm)
k	Turbulent kinetic energy ($m^2 s^{-2}$)
k_f	Thermal conductivity of fluid ($W m^{-1} K^{-1}$)
L	Straight section (mm)
Nu	Nusselt number
p	Pressure drop (pa)
Pr	Prandtl number
Pr_t	Turbulent prandtl number
q_p	Heat flux ($W m^{-2}$)
R	Curvature radius (mm)
Re	Reynolds number ($Re = \rho u_{in} / \mu$)
S	Entropy generation ($W m^{-3} K^{-1}$)
T	Temperature (K)
u, v	Velocities components ($m s^{-1}$)
w	Rib width (mm)
x, y	2-D Cartesian coordinates (mm)

Greek symbols

μ	Dynamic viscosity ($N s m^{-2}$)
μ_t	Turbulent dynamic viscosity ($N s m^{-2}$)
ρ	Density ($kg m^{-3}$)
ε	Dissipation rate of turbulent kinetic energy ($m^2 s^{-3}$)
$\sigma_k, \sigma_\varepsilon$	Empirical constant for turbulence model
Δp	Pressure drop (pa)
Γ	Diffusion coefficient
ξ, η	Body-fitted coordinates

Subscripts

a	average
b	Bulk fluid
eff	effective
f	fluid
in	inlet
p	Plate (surface)
r	rib
s	Smooth surface

Abbreviations

FVM	Finite volume method
PEC	Performance evaluation criteria